

Chemotherapy Response Monitoring of Colorectal Liver Metastases by Dynamic Gd-DTPA-Enhanced MRI Perfusion Parameters and ^{18}F -FDG PET Metabolic Rate

Dennis Vriens¹, Hanneke W.M. van Laarhoven², Jack J.A. van Asten³, Paul F.M. Krabbe⁴, Eric P. Visser¹, Arend Heerschap³, Cornelis J.A. Punt², Lioe-Fee de Geus-Oei¹, and Wim J.G. Oyen¹

¹Department of Nuclear Medicine, Radboud University Nijmegen Medical Centre, Nijmegen, The Netherlands; ²Department of Medical Oncology, Radboud University Nijmegen Medical Centre, Nijmegen, The Netherlands; ³Department of Radiology, Radboud University Nijmegen Medical Centre, Nijmegen, The Netherlands; and ⁴Department of Epidemiology, Biostatistics, and Health Technology Assessment, Radboud University Nijmegen Medical Centre, Nijmegen, The Netherlands

In this study, we examined the in vivo relationship between functional tumor vasculature, determined by dynamic contrast-enhanced (DCE-) MRI, and tumor metabolism, determined by dynamic ^{18}F -FDG PET, during cytotoxic treatment of patients with colorectal liver metastases. **Methods:** Twenty-three patients underwent DCE-MRI (using gadolinium dimeglumine) and dynamic ^{18}F -FDG PET at baseline and after 3 treatment cycles, unless treatment was terminated because of toxicity. Parameters for vasculature (rate constant between extravascular extracellular space and blood plasma [k_{ep}] and volume transfer constant [K^{trans}]), extracellular space (v_e), tumor size (the maximal axial diameter of each included lesion [MAD]), and metabolism (glucose metabolic rates [MR_{glc}]) were derived, and changes during treatment were correlated. Overall survival (OS) and progression-free survival (PFS) served as outcome measures for the predictive abilities of pretreatment parameters and of treatment-related parameter changes. **Results:** Pretreatment MR_{glc} and MAD were individually predictive for OS and PFS. During treatment, K^{trans} increased significantly, but this increase could not be confirmed in a lesion-by-lesion analysis. MR_{glc} decreased significantly ($P < 0.001$). No correlations were found for changes in DCE-MRI parameters and $\Delta\text{MR}_{\text{glc}}$. No relationship was found between changes in DCE-MRI parameters and OS or PFS. $\Delta\text{MR}_{\text{glc}}$ was able to predict OS ($P = 0.008$) after correction for confounders. **Conclusion:** The efficacy of cytotoxic chemotherapy assessed by reduction in tumor metabolism does not depend on pretreatment properties of the tumor vasculature determined by DCE-MRI. Cytotoxic chemotherapy does not alter DCE-MRI-derived properties of tumor vasculature but decreases glucose consumption of tumor cells.

Key Words: colorectal carcinoma; DCE-MRI; ^{18}F -FDG; PET; chemotherapy; therapy monitoring; survival

J Nucl Med 2009; 50:1777–1784
DOI: 10.2967/jnumed.109.064790

Chemotherapy is usually the treatment of choice in patients with advanced colorectal cancer (CRC). Advances in cytotoxic treatment have improved the median survival from 8 mo to more than 20 mo (1). Unfortunately, chemotherapy is only effective in a subset of patients. Early response prediction would enable individualized treatment and prevent side effects and costs due to futile treatment of nonresponders.

The efficacy of chemotherapy depends on the delivery of cytotoxic drugs by the tumor vasculature, uptake and retention of the drug in tumor cells, metabolic activation of prodrugs, intrinsic chemosensitivity of tumor cells, and catabolism and excretion of drugs. Capillary perfusion and permeability of the vessel wall can be measured in vivo by dynamic contrast-enhanced MRI (DCE-MRI) using gadolinium dimeglumine (Gd-DTPA) as the contrast agent (2). Glucose metabolic activity can be assessed in vivo by PET using the radionuclide-labeled glucose analog ^{18}F -FDG (3).

Pharmacokinetic analysis of DCE-MRI data yields parameters for perfused capillaries including blood flow, permeability, and the total surface area. Assuming that vascularity, as reflected by these parameters, is also relevant for the delivery of relatively small cytotoxics to the tumor, it may be hypothesized that these parameters can be used for the prediction of treatment response. The value of baseline DCE-MRI parameters to predict treatment outcome has been shown for several tumor types including CRC (4,5), and its significance in the early monitoring of treatment

Received Apr. 1, 2009; revision accepted Aug. 17, 2009.

For correspondence or reprints contact: Dennis Vriens, Department of Nuclear Medicine, Internal Postal Code 444, Radboud University, Nijmegen Medical Centre, P.O. Box 9101, 6500 HB Nijmegen, The Netherlands.

E-mail: D.Vriens@nuccmed.umcn.nl

COPYRIGHT © 2009 by the Society of Nuclear Medicine, Inc.

response has been shown for rectal (5) and breast (6–8) cancer.

^{18}F -FDG uptake is increased in malignant tumors. An adequate vascular supply and the presence of several membrane-bound glucose transport proteins are necessary for the delivery of glucose to tumor cells, and intracellular hexokinase is necessary for subsequent phosphorylation. ^{18}F -FDG uptake can be quantified by glucose metabolic rates (MR_{glc}) derived from dynamic ^{18}F -FDG PET data. The value of baseline MR_{glc} as a predictive parameter for treatment outcome has been shown for several tumor types, including non-small cell lung carcinoma and CRC (9), and its predictive value using changes in MR_{glc} for the early evaluation of response during chemotherapy has been shown in many tumor types, including non-small cell lung carcinoma (10) and CRC (11).

Because DCE-MRI and ^{18}F -FDG PET assess 2 different determinants of chemotherapy efficacy, their combination could aid in the unraveling of the principles of chemosensitivity. In this prospective study, we investigated the predictive value of pretreatment pharmacokinetic parameters and the value of (early) cytotoxic therapy-induced changes in pharmacokinetic parameters of Gd-DTPA and ^{18}F -FDG with respect to overall survival (OS) and progression-free survival (PFS).

MATERIALS AND METHODS

Patients

Patients with liver metastases of histologically proven CRC who underwent a diagnostic work-up before the start of cytotoxic chemotherapy between June 2002 and September 2005 were eligible. Liver metastases were established during routine staging or during follow-up by abdominal CT ($n = 21$), ultrasound ($n = 1$), or MRI ($n = 1$). Follow-up included a 3-monthly ultrasonography or CT scan. Patients with diabetes mellitus, severe claustrophobia, or implanted electrical devices and with (multiple) small (<1 cm) lesions, in whom the limited spatial resolution of the PET scanner would pose technical difficulties for quantification, were excluded. The study was approved by the institutional review board of the Radboud University Nijmegen Medical Centre, and all patients gave written informed consent.

Thirty-three patients with liver metastases of CRC were included in this prospective study. For 5 patients, DCE-MRI data were not complete because of technical problems ($n = 2$) or the unavailability of a pretherapy scan ($n = 1$) or a follow-up scan ($n = 2$); for 4 patients, ^{18}F -FDG PET data were not complete because of technical problems during the follow-up dynamic acquisition ($n = 1$) or the unavailability of a follow-up scan ($n = 3$). For 1 patient, both DCE-MRI and ^{18}F -FDG PET at follow-up were inaccessible. Therefore, complete datasets of 2 DCE-MRI and two ^{18}F -FDG PET scans were available for 23 patients for analysis of treatment response. Patient characteristics are listed in Table 1. Thirty-one lesions in total could be matched for lesion-by-lesion analysis on MRI (34 lesions visible) and ^{18}F -FDG PET (56 lesions visible because of the larger axial field of view [FOV] of PET than MRI) by 2 experienced observers. In 4 patients, metastases visible on DCE-MRI could not be identified

TABLE 1. Patient Characteristics

Characteristic	Value
No. of patients	23
Demographic	
Mean age (y)	61.5
Range (y)	44.8–78.9
No. of men	17 (74%)
Matched lesions per patient	
Mean	1.3
Range	1–5
Patients > 1 matched lesion	5 (22%)
Median lesion MAD (mm)	56
IQR (mm)	38–75
Histology	
Adenocarcinoma	22 (96%)
Mucinous adenocarcinoma	1 (4%)
Location of primary tumor	
Sigmoid	9 (39%)
Rectum	6 (26%)
Colon	5 (22%)
Colon and rectum	3 (13%)
Presenting stage	
Stage II	3 (13%)
Stage III	4 (17%)
Stage IV	16 (70%)

as separate lesions on ^{18}F -FDG PET. Therefore, the MR_{glc} of the combined lesion was used.

Nine patients received chemotherapy in the first, 11 in the second, 2 in the third, and 1 in fourth lines. The median interval between the last day of the previous-line chemotherapy and the baseline scan for patients treated in the second or higher line was 39 d (interquartile range [IQR], 23–150 d). None of these 14 patients had been treated with antiangiogenic agents before inclusion in the study. The treatment regimens were irinotecan ($n = 7$), capecitabine ($n = 5$), capecitabine/irinotecan ($n = 4$), capecitabine/oxaliplatin ($n = 3$), 5-fluorouracil (5-FU)/folinic acid/oxaliplatin (FOLFOX; $n = 3$), and 5-FU/folinic acid ($n = 1$).

No patients were lost to follow-up. Median OS was 1.5 y (1-, 2-, and 3-y proportions, 70%, 26%, and 9%, respectively), and median PFS was 5.3 mo. At the closeout date, 2 patients were alive (follow-up, 4.3 and 5.6 y, respectively). All patients showed progression of disease.

DCE-MRI and ^{18}F -FDG PET were performed before the start and after 3 cycles of chemotherapy (cycle duration, 21 d, except for FOLFOX, which lasted 14 d). When treatment was terminated before 3 cycles ($n = 6$; range, 0.5–2.0 cycles), the follow-up scan was performed earlier. The median duration of treatment was 50 d (IQR, 30–56 d). The median interval between the last treatment day and the follow-up scan was 6 d (IQR, 2.5–15.5 d).

DCE-MRI

Quantitative DCE-MRI Data Acquisition and Reconstruction. Measurements were performed on a 1.5-T Siemens MRI scanner, using a body phased-array coil. After conventional T1- and T2-weighted imaging, 15 mL of 0.5 M Gd-DTPA (Magnevist; Schering) was administered intravenously at an injection rate of $2.5 \text{ mL}\cdot\text{s}^{-1}$ by a Spectris MR injection system (Medrad Inc.). An axial T1-weighted fast low-angle shot sequence was used to monitor Gd-DTPA uptake in the tumor and the bolus passage in vessels in the spleen (repetition time [TR], 21 ms; echo time [TE],

1.5–1.57 ms; flip angle, 45°; slice thickness, 7 mm, 4–6 slices; matrix size, 256 × 125 pixels; FOV, 284 × 350 mm; total acquisition time, 90 s). The fast acquisition scheme was performed multislice; that is, 4–6 slices were acquired simultaneously within the TR, realized by short TE and short pulse duration. The acquisition matrix was 256 × 125 pixels per slice. Application of the partial Fourier technique (factor, 6/8) reduced the number of phase-encoding steps to 94, which in turn led to a net temporal resolution of 94 × approximately 21 ms = approximately 2 s. If the 4–6 slices in the axial FOV did not fully cover the tumor in the axial direction, slices were positioned in such a way that the largest diameter of the tumor (on the coronal view) was covered. During the acquisition, patients were instructed to breathe quietly and shallowly.

Immediately before the Gd-DTPA injection, proton density-weighted images were recorded with the same sequence parameters as those for the DCE-MRI, except for a flip angle of 10° and a TR of 250 ms. Data from these images were combined with the DCE-MRI data to calculate the concentration of Gd-DTPA in arbitrary units, using the methods described by Hittmair et al. (12).

MRI Data Analysis. For the analysis of DCE-MRI, a vascular normalization function was obtained from pixels in the spleen using an algorithm based on the concentration of Gd-DTPA (high in blood vessels) and time to bolus passage (short in arteries) as described earlier (13). Using a physiologic pharmacokinetic model (14), we analyzed the Gd-DTPA concentration versus time curves of the pixels in all MRI slices (256 × 125 pixels) containing tumor tissue, and the k_{ep} (s^{-1}) of Gd-DTPA uptake was calculated according to the formula $c_t(t) = K^{trans} \cdot e^{-k_{ep} \times t} \otimes c_p(t)$, in which c_t is the tissue concentration of Gd-DTPA, k_{ep} is the rate constant of contrast agent exchange between the extracellular extravascular space and the plasma compartment, K^{trans} is the volume transfer constant between these compartments (s^{-1}), c_p is the concentration of contrast agent in plasma of a capillary, and \otimes denotes a convolution operation (2). In Larsson's model (14), the Gd-DTPA uptake rate constant (k_{ep}) is directly related to tumor blood flow, the product of the permeability, and the total surface area of perfused capillaries, according to $k_{ep} = (1 - e^{-P \times S \times TBF^{-1}}) \times TBF \times v_e^{-1} = K^{trans} \times v_e^{-1}$, in which v_e is the volume of extravascular extracellular space per unit volume of tissue, P is the permeability of capillaries ($cm \cdot s^{-1}$), S is the total surface area of the vessels (cm^2), and TBF is the tumor blood flow ($mL \cdot s^{-1}$). Previous reports have confirmed that there is a moderately strong positive correlation between k_{ep} and microvessel density in liver metastases ($r = 0.458$, $P = 0.037$) (15).

The spatial distribution of the pharmacokinetic parameters was represented as a map. On a T1-weighted MR image recorded directly before Gd-DTPA injection, a region of interest (ROI) was drawn that comprised the metastases. Only large lesions (i.e., >15 mm) that were totally covered by the FOV of the acquired images and were not disturbed by artifacts of inflow of Gd-DTPA in the abdominal aorta (i.e., lesions directly ventral to the aorta) were included. Six lesions were smaller than 30 mm. This ROI was applied to the map of pharmacokinetic parameters to select the single values of k_{ep} , K^{trans} , and v_e for all tumor pixels. Whole-tumor values were calculated after log transformation of all voxels within the ROI, thereby excluding voxels for which k_{ep} , K^{trans} , and $v_e = 0 \text{ s}^{-1}$, which are assumed to represent necrotic tissue or fit artifacts. Mean tumor values and 95% confidence intervals were obtained by backtransformation (13). To obtain a whole-patient value, a mean value, weighted by lesion volume, of all lesions within the FOV was determined by:

$$\text{parameter}_{\text{whole-patient}} = \frac{\sum(\text{parameter}_{\text{lesion}} \times \text{volume}_{\text{lesion}})}{\sum \text{volume}_{\text{lesion}}}$$

The coronal T1-weighted images were used to measure the maximal axial diameter of each included lesion (MAD, in mm) to evaluate morphologic treatment response. Patient-based MADs were calculated by the sum of all included lesions.

¹⁸F-FDG PET

Quantitative Dynamic ¹⁸F-FDG PET Data Acquisition and Reconstruction. Dynamic PET was performed on an ECAT-EXACT 47 dedicated PET scanner (Siemens/CTI) using the ECAT 7.2.1 software for 2-dimensional reconstruction. Patients fasted for at least 6 h before imaging. Intake of sugar-free liquids was permitted. Blood glucose levels (hexokinase method) (Aeroset; Abbott Diagnostics) were determined. The median fasting glucose level was 5.3 mmol·L⁻¹ (maximum, 9.2 mmol·L⁻¹). The location for the dynamic acquisition in the axial FOV (162 mm in 47 planes) of the scanner was based on whole-body ¹⁸F-FDG PET and CT scans obtained for routine clinical work-up, including as many measurable tumor lesions as possible. A 20-min transmission scan was made, using the internal ⁶⁸Ge/⁶⁸Ga sources, to correct for photon attenuation. Approximately 200 MBq (mean ± SD, 202 ± 40 MBq) of ¹⁸F-FDG (Covidien) was injected intravenously using constant infusion by a remote-controlled pump (Medrad Inc.). The dynamic data acquisition, performed in 2-dimensional mode, was started simultaneously with the injection of ¹⁸F-FDG and consisted of 16 time frames with variable duration (10 × 30, 3 × 300, and 3 × 600 s) for a total time of 50 min. During the acquisition, patients were instructed to breathe quietly and shallowly. Correction for decay, randoms, and scatter was performed. Attenuation-corrected images were reconstructed in 128 × 128 matrices using filtered backprojection with a gaussian filter of 4 mm in full width at half maximum. This resulted in forty-seven 3.375-mm slices for each time frame, with voxel dimensions of 3.432 × 3.432 × 3.375 mm and a spatial resolution of 6 mm in full width at half maximum in the reconstructed images.

¹⁸F-FDG PET Data Analysis. ¹⁸F-FDG PET data were analyzed as described before (16). In brief, a plasma time-activity concentration curve was obtained by serial arterial sampling. When arterial sampling was not feasible or was contraindicated, an image-derived input function of the abdominal aorta was used (48% of forty-six ¹⁸F-FDG PET scans). Tumor time-activity concentration curves were obtained by determination of volume-weighted mean activity concentration within ROIs. These ROIs were placed semiautomatically over the metastases using 50% of the maximum voxel value within the lesion on the summed images of frames 14–16 (20–50 min after injection). For therapy response monitoring, the lesion-specific ROI with the largest volume was copied to the other scan (17). Using Patlak graphical analysis (3,18), we determined MR_{glc}, using a lumped constant of 1 and a fractional blood volume of 0. A volume-weighted mean value for all lesions corresponding with DCE-MRI was obtained as patient-based data using the same equation as the one used for DCE-MRI data.

Clinical Follow-Up

Follow-up was performed according to a stringent protocol for 3 y in accordance with standard clinical care. Tumor response for clinical decision making was evaluated by experienced radiologists,

without knowledge of DCE-MRI or dynamic ^{18}F -FDG PET results, according to Response Evaluation Criteria in Solid Tumors (19). Changes in the DCE-MRI parameters (k_{ep} , K^{trans} , v_e), MAD, and ^{18}F -FDG PET parameter MR_{glc} during treatment were calculated as:

$$\Delta\text{parameter} = \left(\text{parameter}_{\text{follow-up}} - \text{parameter}_{\text{baseline}} \right) \times \text{parameter}_{\text{baseline}}^{-1} \times 100\%.$$

The date of progression was defined as the earliest date at which disease progression was confirmed. Survival and progression were measured from the date of baseline ^{18}F -FDG PET or DCE-MRI (whichever was performed first) to the date of, respectively, disease-related death or progression. For patients who were alive ($n = 2$) at the closeout date (May 2009), survival was censored.

The median interval between all DCE-MRI and ^{18}F -FDG PET scans was 0 d (IQR, 0–1 d). The mean interval between the baseline and the first follow-up PET scan was 59.1 ± 11.3 d.

Statistical Analysis

Both patient-based analysis and lesion-by-lesion analysis were performed. DCE-MRI, T1-weighted MRI, and ^{18}F -FDG PET data were analyzed separately, and the results were masked. Variables were assessed for normality by Shapiro–Wilk statistics. Means (\pm SD) for normally distributed data or medians (IQR) are presented. Differences were assessed for significance by the Mann–Whitney U test and by the paired t test (normally distributed) or Wilcoxon signed rank test for paired data. Correlations were determined by the nonparametric Spearman ρ .

Cancer-related OS and PFS were calculated using Kaplan–Meier estimates. Both univariate and multivariate analyses were performed by the Cox proportional hazards model. The relationship between DCE-MRI and ^{18}F -FDG PET parameters and OS and PFS was assessed for both pretreatment values (predictive value of tumor parameters) and changes in parameter values during treatment (predictive value of early treatment response). Separate (univariate) analysis was performed for the relationship between OS and PFS and the following covariates: number of lesions, patient age, TNM classification, tumor differentiation, histology or localization, chemotherapy line (first line vs. second or higher lines), and regimen and the number of chemotherapy cycles before the follow-up scan. Hazard ratios (HRs) are presented with their 95% confidence intervals (Wald χ^2 test). Multivariate analysis was performed using imaging parameters and significant covariates in a backwardly designed conditional Cox proportional hazards model, removing variables when P was greater than 0.100.

All statistical analyses were performed with SPSS software (version 16.0.2 for Mac; SPSS Inc.). Statistical tests were based on a 2-sided significance level set at $P = 0.050$ for all tests.

RESULTS

Predictive Value of Pretreatment DCE-MRI and ^{18}F -FDG PET

An example of DCE-MRI and ^{18}F -FDG PET data is displayed in Figure 1. No statistically different pretreatment parameters for tumor size and vascular parameters were found for patients who were treated in the first line ($n = 9$) versus patients who had been treated with cytotoxic therapy

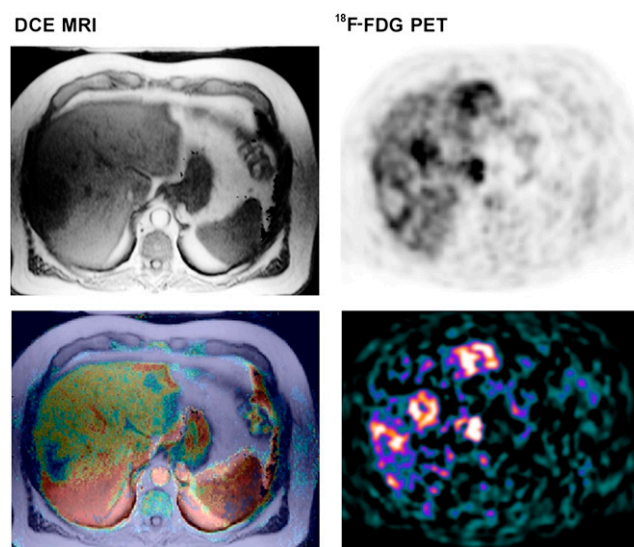


FIGURE 1. Example of 78-y-old man with intermediately differentiated adenocarcinoma of sigmoid ($T_3N_1M_1$) with metachronous liver metastases. (Left, top to bottom) Conventional T1-weighted MR image (before Gd-DTPA) and fused parametric image of k_{ep} values with T1-weighted MR image. (Right, top to bottom) ^{18}F -FDG PET uptake image (20–50 min after injection) and parametric image of MR_{glc} .

previously ($n = 14$). MR_{glc} was slightly lower in the patients who were treated in the first line. This, however, did not reach significance (median MR_{glc} , $0.1095 \mu\text{mol}\cdot\text{mL}^{-1}\cdot\text{min}^{-1}$ vs. $0.1373 \mu\text{mol}\cdot\text{mL}^{-1}\cdot\text{min}^{-1}$, $P = 0.072$).

Patient-based analysis of the pretreatment scans showed a significant positive correlation between the tumor size (MAD) and the fraction of extravascular extracellular space (v_e) ($\rho = 0.426$, $P = 0.043$). Neither the patient-based analysis nor the lesion-by-lesion analysis yielded significant correlations between pretreatment DCE-MRI and ^{18}F -FDG PET parameters. The correlation between baseline k_{ep} and MR_{glc} was -0.028 ($P = 0.880$).

Univariate Cox regression analysis established an OS and PFS benefit in patients with low baseline MR_{glc} values. Baseline MAD showed a minor but significant relationship with OS as well, but chemotherapy line (first line vs. higher lines) showed no significant relationship with either OS or PFS in this group of patients. None of the DCE-MRI parameters for vascularity showed a significant relationship with either OS or PFS. When these variables were used in multivariate analysis, correction for MAD increased the HR of MR_{glc} for OS and PFS, but additional correction for chemotherapy line did not improve the predictive ability of the model as a whole (Table 2).

Lesion-by-Lesion Analysis of Changes in Scan Parameters

A significant change in median MR_{glc} ($0.138 \mu\text{mol}\cdot\text{mL}^{-1}\cdot\text{min}^{-1}$ to $0.059 \mu\text{mol}\cdot\text{mL}^{-1}\cdot\text{min}^{-1}$, $P < 0.001$) was found at the follow-up, but no significant changes were

TABLE 2. Predictive Value of Pretreatment Parameters to Survival Assessed by Cox Regression Analysis

Parameter	OS			PFS		
	HR	CI	<i>P</i>	HR	CI	<i>P</i>
Univariate						
MR _{glc} [*]	3.61	1.58–8.26	0.002 [†]	3.11	1.41–6.86	0.005 [†]
MAD [‡]	1.03	1.00–1.06	0.032 [†]	1.03	1.00–1.07	0.039 [†]
Chemotherapy line [§]	2.19	0.87–5.51	0.097	2.40	0.96–6.03	0.062
Multivariate						
MR _{glc} [*]	4.29	1.72–10.67	0.002 [†]	3.19	1.39–7.35	0.006 [†]
MAD [‡]	1.04	1.01–1.07	0.020 [†]	1.03	1.00–1.07	0.059
Chemotherapy line [§]	—	—	—	—	—	—

^{*}Per 0.1 μmol·mL⁻¹·min⁻¹ change.
[†]Significant (*P* > 0.05) assessed by Wald's χ² test.
[‡]Per 5-mm change.
[§]First-line vs. higher lines.
 CI = 95% confidence interval.

seen in the other parameters. K^{trans} did not change significantly ($P = 0.088$). No correlations were present between changes in ¹⁸F-FDG PET parameters and changes in DCE-MRI parameters during treatment.

Predictive Value of Changes in DCE-MRI and ¹⁸F-FDG PET Parameters

For response to chemotherapy, no statistical differences were seen between the changes in tumor size, DCE-MRI vascularity parameters, and MR_{glc}, between the group that was treated with systemic treatment in the first line ($n = 9$) and the group that was treated in higher lines ($n = 14$) (all $P > 0.305$).

Results of scan parameters before and after the start of treatment are provided in Table 3. There was a significant change in both MR_{glc} (median baseline, 0.128 μmol·mL⁻¹·min⁻¹ to 0.054 μmol·mL⁻¹·min⁻¹ at follow-up, $P < 0.001$) and K^{trans} (median baseline, 0.009 s⁻¹ to 0.016 s⁻¹ at follow-up, $P = 0.035$) during chemotherapy. No significant correlations were found between parameter changes during treatment. The correlation between ΔK^{trans} and $\Delta \text{MR}_{\text{glc}}$ was $\rho = -0.172$ ($P = 0.433$).

To assess whether preexisting vasculature as assessed by DCE-MRI influenced therapy response by delivery of cytotoxic drugs, k_{ep} before chemotherapy was correlated to metabolic and anatomic response, but no significant relationship could be established between k_{ep} and ΔMAD ($\rho = -0.209$, $P = 0.340$) or $\Delta \text{MR}_{\text{glc}}$ ($\rho = 0.257$, $P = 0.237$). The same applied for K^{trans} and v_e . In lesion-by-lesion analysis, k_{ep} before chemotherapy was not correlated with ΔMAD ($\rho = -0.197$, $P = 0.289$) or $\Delta \text{MR}_{\text{glc}}$ ($\rho = 0.293$, $P = 0.109$).

Univariate Cox regression analysis showed no relationship of any change in DCE-MRI or ¹⁸F-FDG PET parameters with respect to OS. When all lesions inside the larger FOV of the PET scanner were quantified (instead of only the matching lesions) to determine a patient-based MR_{glc}, $\Delta \text{MR}_{\text{glc}}$ was predictive for OS (HR, 1.15; $P = 0.041$). Only ΔMAD was related to both OS (HR, 1.40; $P = 0.023$) and PFS (HR, 1.34; $P = 0.026$). Chemotherapy line was not a significant confounder for OS or PFS. Multivariate Cox regression modeling showed both $\Delta \text{MR}_{\text{glc}}$ (HR, 1.22; $P = 0.008$) and Δk_{ep} (HR, 0.99; $P = 0.100$) as predictors for OS, but the latter was irrelevantly small. For PFS, both ΔMAD (HR, 1.48; $P = 0.010$) and chemotherapy line (HR,

TABLE 3. Baseline and Follow-up Values of Vascular and Metabolic Parameters ($n = 23$ Patients)

Parameter	Baseline		Follow-up		<i>P</i>
	Median	IQR	Median	IQR	
DCE-MRI					
k_{ep} (s ⁻¹)	0.014	0.005–0.034	0.022	0.012–0.049	0.056
K^{trans} (s ⁻¹)	0.009	0.003–0.020	0.016	0.008–0.033	0.035 [*]
v_e	0.638	0.516–0.698	0.614	0.566–0.744	0.893
¹⁸F-FDG PET					
MR _{glc} (μmol·mL ⁻¹ ·min ⁻¹)	0.128	0.108–0.160	0.054	0.041–0.122	<0.001 [*]
T1-weighted MRI					
MAD (mm)	56	50–92	54	47–109	0.268

^{*} $P < 0.05$ (Wilcoxon signed rank test for paired samples).

3.15; $P = 0.023$) were of predictive relevance. Results are shown in Table 4.

DISCUSSION

Pretreatment Parameters for Vascularity and Metabolism

No association was seen between vascularity, assessed by DCE-MRI, and glucose metabolism, assessed by ^{18}F -FDG PET. Our results confirm those of Brix et al. (20), who found no correlation between k_{ep} and ^{18}F -FDG uptake (standardized uptake value [SUV]) in breast cancer. Semple et al. (21), however, found a positive correlation between k_{ep} and SUV ($\rho = 0.5$) and a positive, though nonsignificant, correlation between K^{trans} and SUV in breast carcinoma patients before the commencement of treatment. They suggested that ^{18}F -FDG delivery was restricted by the blood flow dynamics of the tumor. In a previous study (15), we found a negative correlation between k_{ep} and ^{18}F -FDG uptake (tumor-to-nontumor ratios) in CRC.

The different relationships between vascular and metabolic tumor parameters described in the literature could imply that tumor vasculature is not related to MR_{glc} . However, a more complex relationship between vasculature and MR_{glc} , mediated by acute and chronic tumor hypoxia, could also play a role: Chronic hypoxia and diminished delivery of glucose could be caused by a low blood flow, a low permeability, or a small surface area of tumor blood vessels resulting in low values for k_{ep} . All these vascular parameters may result in a decreased supply of nutrients such as glucose and oxygen to the tumor, similar to the decreased delivery of Gd-DTPA, which would lead to decreased cell proliferation as an energy-saving method (22) or to necrosis or apoptosis. This situation would result in a positive correlation between k_{ep} and MR_{glc} . Conversely, (transient) hypoxia due to poor vascular function (as measured by a low value for k_{ep}) might induce higher

glucose uptake in the tumor for anaerobic glycolysis (15,23,24). The latter explanation would result in a negative correlation between k_{ep} and MR_{glc} . Therefore, the opposite, combined, complex effects of acute and chronic hypoxia and nutrient supply could explain the lack of correlation between k_{ep} and MR_{glc} . Another reason for this lack of correlation could be nonspecificity of K^{trans} and k_{ep} , which may represent flow, vessel permeability, or surface area or a combination of these. Finally, imprecision in the determination of the DCE-MRI or PET parameters combined with the limited study size might explain the lack of correlation.

Both pretreatment tumor metabolism (MR_{glc}) and size (MAD) were associated with higher hazards for death and progression. This confirms previous data (9), which showed that a 1-unit increase in SUV results in a 17% increase in the risk of death. Multivariate analysis showed no influence of chemotherapy line (first- vs. higher-line treatment) for the predictive abilities of MR_{glc} and MAD.

Previously, Semple et al. (25) had observed a significant correlation ($P < 0.05$) between pretreatment k_{ep} and ΔSUV during chemotherapy of 17 breast cancer patients and concluded that the reduction of measured metabolism may be partly attributable to pretherapy vascular delivery (k_{ep}). Because Gd-DTPA and phenylacetate (which has a size similar to 5-FU) are similarly distributed in the interstitium of tumor tissue (26), a restriction of Gd-DTPA delivery to the interstitium reflects a restriction of 5-FU delivery to the immediate neighborhood of tumor cells. We could not confirm these findings in patients with CRC.

Early Changes in Metabolic and Vascularity Parameters During Treatment

We have found no significant treatment-induced changes in k_{ep} , v_e , and MAD, whereas MR_{glc} and K^{trans} , respectively, significantly decreased and increased on a patient level. On a lesion level, the increase in K^{trans} could not be

TABLE 4. Predictive Value of Therapy-Induced Parameter Changes for Early Response Evaluation, Assessed by Cox Regression Analysis

Parameter	OS			PFS		
	HR	CI	P^*	HR	CI	P^*
Univariate						
$\Delta\text{MR}_{\text{glc}}$ (all in FOV) [†]	1.15	1.01–1.32	0.041	—	—	—
ΔMAD [†]	1.40	1.06–1.85	0.023	1.34	1.04–1.74	0.026
Chemotherapy line [‡]	—	—	—	—	—	—
Multivariate						
$\Delta\text{MR}_{\text{glc}}$ (all in FOV) [†]	1.22	1.05–1.41	0.008	—	—	—
Δk_{ep} [†]	0.99	0.98–1.00	0.100	—	—	—
ΔMAD [†]	—	—	—	1.48	1.10–1.99	0.010
Chemotherapy line [‡]	—	—	—	3.15	1.17–8.49	0.023

*Significance assessed by Wald χ^2 test.

[†]Per 10% change.

[‡]First line vs. higher lines.

CI = 95% confidence interval; all in FOV = estimated including all lesions in FOV of PET scanner.

reproduced. Our results suggest that the observed reduction in MR_{glc} during chemotherapy cannot be explained by changes in tumor vasculature (Δk_{ep}). The antivascular effect of cytotoxic drugs is small and marginally influences cell metabolism and patient survival. It seems that direct cytotoxic effects leading to necrosis and apoptosis cause disease response and improved survival and that possible effects of chemotherapeutic agents on nutrient delivery play a minor role.

The reduction in k_{ep} during therapy has been described in breast cancer (27,28), and reduction in K^{trans} during treatment has been described in rectal (5) and breast (6,7,29) cancer. Some authors explained these changes by the direct antivascular effect of the cytotoxic drugs (7,29) or by the loss of immature tumor vessels (5). Our results, however, do not suggest an effect of cytotoxic drugs on tumor vasculature in CRC.

We found no relationship between vascular parameters and clinical outcome. This confirms the results of our previous study showing no evident relevance of pretreatment k_{ep} , K^{trans} , or v_e for OS and PFS in colorectal liver metastases or any change in these parameters during first-line chemotherapy (30). In the present study, we observed a positive relationship between ΔMR_{glc} and hazards for death but not for progression, which was mainly predicted by chemotherapy line and ΔMAD .

Because DCE-MRI and ^{18}F -FDG PET both address different aspects of tumor physiology, they might be used complementarily in treatment-response evaluation. The choice for a specific imaging modality should depend on the treatment regimen. The cytotoxic drugs given to our patients interfere with DNA synthesis and stabilization, eventually leading to cell death. Therefore, the direct interaction with tumor vascularity is limited, as is suggested by our data, showing no change in DCE-MRI parameters during cytotoxic treatment. When antiangiogenic drugs are used, response might be predicted by DCE-MRI, as shown by 2 studies (31,32) in clear cell renal cell carcinoma patients treated with sorafenib. Response might be monitored by DCE-MRI, showing a decrease of k_{ep} (33), but results are still contradictory (32). The effect of cytotoxic drugs on cell metabolism can be monitored by ^{18}F -FDG PET. Tumor metabolic response has predictive value (11), which is also shown by our data. Early disease-related deaths did occur in the group of metabolic responders. Therefore, a reduction in metabolism during therapy does not guarantee a long survival, and more effects presumably play a role.

Study Limitations

Patients were treated in different lines of chemotherapy using different chemotherapy regimens; thus, the included population was heterogeneous. Furthermore, currently combinations of cytotoxic treatment with antiangiogenic treatment are standard in first-line treatment. DCE-MRI may have a role as a tool for response evaluation in those

patients who are being treated with antiangiogenics. Previous chemotherapy might already have influenced both metabolism and vascularity. However, subgroup analysis of the 9 patients treated with first-line chemotherapy did not change our conclusions.

Only a selection of lesions could be analyzed because of the limited FOV of the acquired images and the limited spatial resolution of (especially) the PET system, which might have caused some bias during selection.

The parameters for vascularity as derived from DCE-MRI were not verified by histologic quantification of microvessel density, because biopsies of stage IV patients are taken only in exceptional circumstances. However, we have previously described a relationship between both histology and DCE-MRI parameters (15). An advantage of DCE-MRI over histology is that DCE-MRI measures functional vasculature only, whereas the quantification of histologic staining of endothelial cells also includes non-perfused vessels.

CONCLUSION

Dynamic Gd-DTPA-enhanced MRI parameters of tumor vasculature showed no relationship to tumor metabolic response on dynamic ^{18}F -FDG PET or to patient survival during cytotoxic chemotherapy either before or during treatment. Therefore, a decrease in metabolic activity and an increase in OS and PFS during chemotherapy cannot be attributed to changes in tumor vascularity, resulting in the altered delivery of drugs or nutrients of the same size as Gd-DTPA. The present study underlines the potential of ^{18}F -FDG PET for response monitoring. The main conclusions of the article are valid for patients not receiving vascular-targeted therapy, and further study is required in the subset of patients who do receive additional antiangiogenic agents.

ACKNOWLEDGMENTS

This study was presented at the 56th annual meeting of the Society of Nuclear Medicine, Toronto, Ontario, Canada, June 15, 2009.

REFERENCES

1. Punt CJ. New options and old dilemmas in the treatment of patients with advanced colorectal cancer. *Ann Oncol*. 2004;15:1453–1459.
2. Tofts PS, Brix G, Buckley DL, et al. Estimating kinetic parameters from dynamic contrast-enhanced T_1 -weighted MRI of a diffusible tracer: standardized quantities and symbols. *J Magn Reson Imaging*. 1999;10:223–232.
3. Patlak CS, Blasberg RG, Fenstermacher JD. Graphical evaluation of blood-to-brain transfer constants from multiple-time uptake data. *J Cereb Blood Flow Metab*. 1983;3:1–7.
4. Devries AF, Griebel J, Kremser C, et al. Tumor microcirculation evaluated by dynamic magnetic resonance imaging predicts therapy outcome for primary rectal carcinoma. *Cancer Res*. 2001;61:2513–2516.
5. George ML, Dzik-Jurasz AS, Padhani AR, et al. Non-invasive methods of assessing angiogenesis and their value in predicting response to treatment in colorectal cancer. *Br J Surg*. 2001;88:1628–1636.
6. Pickles MD, Lowry M, Manton DJ, Gibbs P, Turnbull LW. Role of dynamic contrast enhanced MRI in monitoring early response of locally advanced

- breast cancer to neoadjuvant chemotherapy. *Breast Cancer Res Treat.* 2005;91:1–10.
7. Delille JP, Slanetz PJ, Yeh ED, Halpern EF, Kopans DB, Garrido L. Invasive ductal breast carcinoma response to neoadjuvant chemotherapy: noninvasive monitoring with functional MR imaging pilot study. *Radiology.* 2003;228:63–69.
 8. Thukral A, Thomasson DM, Chow CK, et al. Inflammatory breast cancer: dynamic contrast-enhanced MR in patients receiving bevacizumab—initial experience. *Radiology.* 2007;244:727–735.
 9. de Geus-Oei LF, Wiering B, Krabbe PF, Ruers TJ, Punt CJ, Oyen WJ. FDG-PET for prediction of survival of patients with metastatic colorectal carcinoma. *Ann Oncol.* 2006;17:1650–1655.
 10. de Geus-Oei LF, van der Heijden HF, Visser EP, et al. Chemotherapy response evaluation with ¹⁸F-FDG PET in patients with non-small cell lung cancer. *J Nucl Med.* 2007;48:1592–1598.
 11. de Geus-Oei LF, van Laarhoven HW, Visser EP, et al. Chemotherapy response evaluation with FDG-PET in patients with colorectal cancer. *Ann Oncol.* 2008;19:348–352.
 12. Hittmair K, Gomiscek G, Langenberger K, Recht M, Imhof H, Kramer J. Method for the quantitative assessment of contrast agent uptake in dynamic contrast-enhanced MRI. *Magn Reson Med.* 1994;31:567–571.
 13. van Laarhoven HW, Rijpkema M, Punt CJ, et al. Method for quantitation of dynamic MRI contrast agent uptake in colorectal liver metastases. *J Magn Reson Imaging.* 2003;18:315–320.
 14. Larsson HB, Stubgaard M, Frederiksen JL, Jensen M, Henriksen O, Paulson OB. Quantitation of blood-brain barrier defect by magnetic resonance imaging and gadolinium-DTPA in patients with multiple sclerosis and brain tumors. *Magn Reson Med.* 1990;16:117–131.
 15. van Laarhoven HW, de Geus-Oei LF, Wiering B, et al. Gadopentetate dimeglumine and FDG uptake in liver metastases of colorectal carcinoma as determined with MR imaging and PET. *Radiology.* 2005;237:181–188.
 16. de Geus-Oei LF, Visser EP, Krabbe PF, et al. Comparison of image-derived and arterial input functions for estimating the rate of glucose metabolism in therapy-monitoring ¹⁸F-FDG PET studies. *J Nucl Med.* 2006;47:945–949.
 17. Vriens D, de Geus-Oei LF, van Laarhoven HWM, et al. Comparison of two region of interest definition methods for metabolic response evaluation with [¹⁸F]FDG-PET. *Q J Nucl Med Mol Imaging.* 2009;53:224–244.
 18. Willemsen AT, van den Hoff J. Fundamentals of quantitative PET data analysis. *Curr Pharm Des.* 2002;8:1513–1526.
 19. Therasse P, Arbuck SG, Eisenhauer EA, et al. New guidelines to evaluate the response to treatment in solid tumors. European Organization for Research and Treatment of Cancer, National Cancer Institute of the United States, National Cancer Institute of Canada. *J Natl Cancer Inst.* 2000;92:205–216.
 20. Brix G, Henze M, Knopp MV, et al. Comparison of pharmacokinetic MRI and [¹⁸F] fluorodeoxyglucose PET in the diagnosis of breast cancer: initial experience. *Eur Radiol.* 2001;11:2058–2070.
 21. Semple SI, Gilbert FJ, Redpath TW, et al. The relationship between vascular and metabolic characteristics of primary breast tumours. *Eur Radiol.* 2004;14:2038–2045.
 22. Evans SM, Hahn SM, Magarelli DP, Koch CJ. Hypoxic heterogeneity in human tumors: EF5 binding, vasculature, necrosis, and proliferation. *Am J Clin Oncol.* 2001;24:467–472.
 23. Burgman P, Odonoghue JA, Humm JL, Ling CC. Hypoxia-induced increase in FDG uptake in MCF7 cells. *J Nucl Med.* 2001;42:170–175.
 24. Clavo AC, Brown RS, Wahl RL. Fluorodeoxyglucose uptake in human cancer cell lines is increased by hypoxia. *J Nucl Med.* 1995;36:1625–1632.
 25. Semple SI, Staff RT, Heys SD, et al. Baseline MRI delivery characteristics predict change in invasive ductal breast carcinoma PET metabolism as a result of primary chemotherapy administration. *Ann Oncol.* 2006;17:1393–1398.
 26. Artemov D, Solaiyappan M, Bhujwalla ZM. Magnetic resonance pharmacokinetics to detect and predict chemotherapy delivery to solid tumors. *Cancer Res.* 2001;61:3039–3044.
 27. Wasser K, Klein SK, Fink C, et al. Evaluation of neoadjuvant chemotherapeutic response of breast cancer using dynamic MRI with high temporal resolution. *Eur Radiol.* 2003;13:80–87.
 28. Wasser K, Sinn HP, Fink C, et al. Accuracy of tumor size measurement in breast cancer using MRI is influenced by histological regression induced by neoadjuvant chemotherapy. *Eur Radiol.* 2003;13:1213–1223.
 29. Hayes C, Padhani AR, Leach MO. Assessing changes in tumour vascular function using dynamic contrast-enhanced magnetic resonance imaging. *NMR Biomed.* 2002;15:154–163.
 30. van Laarhoven HW, Klomp DW, Rijpkema M, et al. Prediction of chemotherapeutic response of colorectal liver metastases with dynamic gadolinium-DTPA-enhanced MRI and localized ¹⁹F MRS pharmacokinetic studies of 5-fluorouracil. *NMR Biomed.* 2007;20:128–140.
 31. Flaherty KT, Rosen MA, Heitjan DF, et al. Pilot study of DCE-MRI to predict progression-free survival with sorafenib therapy in renal cell carcinoma. *Cancer Biol Ther.* 2008;7:496–501.
 32. Hahn OM, Yang C, Medved M, et al. Dynamic contrast-enhanced magnetic resonance imaging pharmacodynamic biomarker study of sorafenib in metastatic renal carcinoma. *J Clin Oncol.* 2008;26:4572–4578.
 33. Wedam SB, Low JA, Yang SX, et al. Antiangiogenic and antitumor effects of bevacizumab in patients with inflammatory and locally advanced breast cancer. *J Clin Oncol.* 2006;24:769–777.



The Journal of
NUCLEAR MEDICINE

Chemotherapy Response Monitoring of Colorectal Liver Metastases by Dynamic Gd-DTPA-Enhanced MRI Perfusion Parameters and ^{18}F -FDG PET Metabolic Rate

Dennis Vriens, Hanneke W.M. van Laarhoven, Jack J.A. van Asten, Paul F.M. Krabbe, Eric P. Visser, Arend Heerschap, Cornelis J.A. Punt, Lioe-Fee de Geus-Oei and Wim J.G. Oyen

J Nucl Med. 2009;50:1777-1784.
Published online: October 16, 2009.
Doi: 10.2967/jnumed.109.064790

This article and updated information are available at:
<http://jnm.snmjournals.org/content/50/11/1777>

Information about reproducing figures, tables, or other portions of this article can be found online at:
<http://jnm.snmjournals.org/site/misc/permission.xhtml>

Information about subscriptions to JNM can be found at:
<http://jnm.snmjournals.org/site/subscriptions/online.xhtml>

The Journal of Nuclear Medicine is published monthly.
SNMMI | Society of Nuclear Medicine and Molecular Imaging
1850 Samuel Morse Drive, Reston, VA 20190.
(Print ISSN: 0161-5505, Online ISSN: 2159-662X)

© Copyright 2009 SNMMI; all rights reserved.

The logo for the Society of Nuclear Medicine and Molecular Imaging (SNMMI) features the letters 'S', 'N', 'M', and 'I' in a stylized, overlapping arrangement. The 'S' and 'N' are in the top row, and the 'M' and 'I' are in the bottom row. The letters are white with a red outline, set against a red background.
SOCIETY OF
NUCLEAR MEDICINE
AND MOLECULAR IMAGING